Phys. Status Solidi A **207**, No. 4, 858–863 (2010) / **DOI** 10.1002/pssa.200983319

physica status solidi a
www.pss-a.com
applications and materials science

Large scale synthesis of single crystalline tungsten nanowires with extreme aspect ratios

Achim Walter Hassel[*,1,2], **Srdjan Milenkovic**[1,2], **and Andrew Jonathan Smith**[1,3]

[1] Max-Planck-Institut für Eisenforschung, Max-Planck-Str. 1, 40237 Düsseldorf, Germany
[2] Institute for Chemical Technology of Inorganic Materials, Johannes Kepler University, Altenberger Str. 69, 4040 Linz, Austria
[3] Kleindiek Nanotechnik GmbH, Aspenhausstr. 25, 72770 Reutlingen, Germany

Received 2 August 2009, revised 17 January 2010, accepted 19 January 2010
Published online 29 March 2010

Keywords nanowires, metals, growth from melts, phase diagram, electrodeposition

* Corresponding author: e-mail hassel@elchem.de, Phone: +43 732 2468 8704, Fax: +43 732 2468 8905

One gram of tungsten nanowires – equivalent to 5 billion single wires – was produced by electrochemically processing a directionally solidified eutectic NiAl-W alloy. Their release is realised by selective dissolution of the matrix with a yield beyond 98%. The nanowires are single crystals, homogeneous in diameter, and have extremely high aspect-ratios (>1000!). A multitude of potential applications are feasible – including sensing, probing, and high temperature nanotechnology.

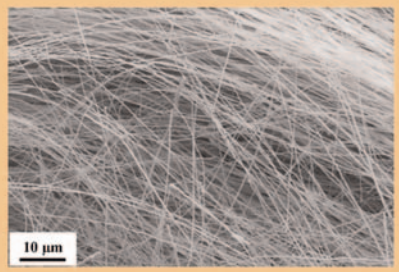

1 Introduction Metal nanowires with their unprecedented physical and mechanical properties are attracting intense research interest. The use of single crystalline nanowires allows reaching the theoretical limits in mechanical strength, electrical, and heat conductivity. Various methods have been developed to fabricate tungsten nanowires. Thong et al. [1] obtained single tungsten nanowires by field-emission induced growth in the presence of tungsten carbonyl as a precursor. Electron emission from the newly grown nanowire tip continued the growth and gave rise to nanowires that are tens of microns long. Nanowires have been grown on carbon nanotubes [2], AFM tips [3], and between two microtip electrodes [4]. Li et al. [5] used pyrolysis and carbothermal reduction of lamellar composites of tungsten oxide with cetyltrimethylammonium bromide (CTAB) in vacuum between 500 and 850 °C to produce metallic W nanowires with diameters in the range of 20–80 nm and lengths 5–30 µm. Hydrothermal treatment of lamellar surfactant/inorganic composite precursors also yielded crystalline metal nanowires [6]. Liu et al. [7, 8] investigated features and growth behavior of self-supporting tungsten nanowire fabricated by electron-beam-induced deposition using 200 keV electrons. Wang et al. [9] synthesized single crystalline tungsten nanowires by a nickel-catalyzed vapor-phase method controlled by vapor–solid–solid mechanism. Also, Lee et al. [10] reported on the field emission properties of nanosized straight tungsten wires fabricated by annealing of W film which behaves as self-catalytic layer. Finally, Ross et al. [11] fabricated amorphous tungsten nanowires by electron and ion beam induced chemical vapor deposition. However, all these methods fail to enable large scale synthesis of single crystalline tungsten nanowires.

High aspect ratio, single crystalline nanowires with homogenous diameters can be obtained in large amounts by utilizing directional solidification of eutectic alloys yielding self-organized nanostructured material. This is typically performed using a Bridgman type oven. The oven consists of two zones – a hot zone and a cold zone. The sample is placed in the hot zone and the alloy is allowed to melt completely. Then the sample is lowered into the cold zone with a well-defined, constant speed. Segregation of the phases during solidification is diffusion controlled and yields single crystalline nanoscopic metal wires embedded in a single crystalline metal matrix. The diameter and spacing of the wires can be influenced by controlling the pulling speed and the temperature gradient between the hot and cold zones [12–15]. The alloy used in this work was NiAl-W yielding tungsten wires inside a nickel–aluminium matrix.

2 Experiments The pre-alloy was prepared by induction melting and casting of metal powders in a water cooled copper mold. Nickel and aluminium were always used in equiatomic amounts. The amount of tungsten was 1.5 at.%. Nickel was obtained from Gesellschaft für Elektrometallurgie, Nürnberg, Germany, aluminium from VAW Aluminium AG, Bonn, Germany, and tungsten from Goodfellow GmbH, Friedberg, Germany. It was subsequently processed in a Bridgman-type crystal growth oven at a temperature gradient of 40 K cm^{-1} and growth rate of 30 mm h^{-1}.

In order to access the nanowires it is necessary to selectively dissolve the matrix phase. Studying the Pourbaix diagrams for the involved elements allowed determining the proper chemical and electrochemical conditions for dissolving nickel and aluminium while simultaneously passivating tungsten [16]. The chosen conditions were 1 M hydrochloric acid and an applied potential of 200 mV (SHE). Electrochemical measurements were performed using an IviumStat potentiostat (Ivium Technologies, Eindhoven, The Netherlands) in combination with a commercial Ag | AgCl | 3 M KCl reference electrode (Deutsche Metrohm GmbH & Co, Filderstadt, Germany).

Handling of the nanowires was performed using Kleindiek manipulation system consisting of piezo driven manipulator (MM3A-EM) and a piezo driven gripper (MGS2-EM) – each with sub-nanometer precision – manufactured by Kleindiek Nanotechnik GmbH. The manipulators were equipped with standard tool tip, so-called picoprobes. These probes consist of a tinned copper shaft (0.51 mm) to which a 10 μm tungsten wire is attached. The tungsten wire has a pointed tip with a nominal diameter <0.1 μm (GGB Industries, Inc., Naples, FL, USA).

3 Results and discussion

3.1 Large scale synthesis Processing the samples electrochemically proved to be highly selective as can be seen from Fig. 1 in which the nanowires exposed by this method retain their cylindrical shape. The diameter was homogeneous along the wire, whereas the scattering for the different wires was quite narrow [17]. Therefore, this method was employed for scaling up the process in order to mass produce W nanowires, as shown schematically in Fig. 2. The initial goal was to produce the benchmark value of 1 g of tungsten nanowires.

Considering that the alloy contains 6.1 wt% of W, it was calculated that 21.3 g of alloy is necessary to yield approximately 1 g of W nanowires. Assuming the following anodic reactions:

$$\mathrm{Al} \rightarrow \mathrm{Al}^{3+} + 3\mathrm{e}^- \quad \text{and} \quad \mathrm{Ni} \rightarrow \mathrm{Ni}^{2+} + 2\mathrm{e}^-, \tag{1}$$

as well as cathodic reaction:

$$2\mathrm{H}^+ + 2\mathrm{e}^- \rightarrow \mathrm{H}_2, \tag{2}$$

it is obvious that for each mole of NiAl that is to be dissolved five electrons are produced and therefore 5 mol of H^+-ions are consumed.

A calculation of the amount of hydrochloric acid required in order to process 20 g of NiAl contained in 21.3 g of *ds*-NiAl-W was performed.

Figure 1 SEM image of tungsten nanowire array. Partially exposed wires protrude from the NiAl matrix. The nanowires' diameter is 200 nm, exposed length is 20 μm.

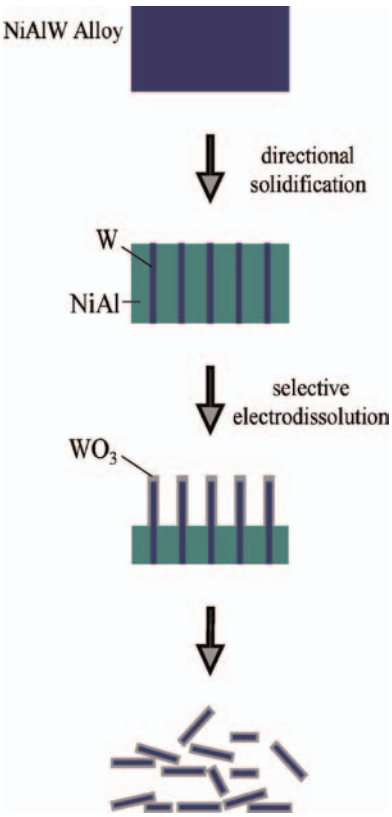

Figure 2 (online color at: www.pss-a.com) Schematic of the process steps for producing either nanowire arrays (Fig. 1) or free wires as shown in Fig. 4.

The molar mass of NiAl is the sum of the molar masses of Ni and Al [18]:

$$M(\mathrm{NiAl}) = M(\mathrm{Ni}) + M(\mathrm{Al}), \tag{3}$$

$$M(\mathrm{NiAl}) = 58.69 + 26.98\,\mathrm{g\,mol^{-1}}. \tag{4}$$

The number of moles of NiAl, Ni, and Al is given by:

$$n(\mathrm{NiAl}) = \frac{m(\mathrm{NiAl})}{M(\mathrm{NiAl})}, \tag{5}$$

$$n(\mathrm{NiAl}) = \frac{20\,\mathrm{g}}{85.68\,\mathrm{g\,mol^{-1}}} = 0.2334\,\mathrm{mol}, \tag{6}$$

$$n(\mathrm{NiAl}) = n(\mathrm{Ni^{2+}}) = n(\mathrm{Al^{3+}}), \tag{7}$$

$$n(\mathrm{Ni^{2+}}, \mathrm{Al^{3+}}) = n(\mathrm{Ni^{2+}}) + n(\mathrm{Al^{3+}}) = 0.4668\,\mathrm{mol}. \tag{8}$$

Equation (8) shows that the total number of moles of cations that are produced when processing this amount of material is 0.4668 mol. Due to the stoichiometry of the reactions mentioned above this number must be multiplied by a factor of 5 resulting in 2.334 mol of H^+. From that number the amount of 1 M hydrochloric acid necessary for dissolving the matrix completely was calculated to be 2.334 l. In order to accommodate this amount of electrolyte a temperature controlled electrochemical cell with a total volume of 2.5 l was employed as depicted in Fig. 3.

It was fitted with a gas inlet to allow purging the electrolyte with argon. Since processing these large amounts of material required many hours of polarization, the Luggin-capillary which connected the commercial Ag | AgCl | 3 M KCl – reference electrode to the cell was filled with an electrolyte (sat. KCl), which was solidified with agar [19]. This prevented blockage of the Luggin-capillary by hydrogen bubbles. A large Pt net was employed as a counter electrode. The pieces of directionally solidified NiAl-W were placed in a Pt basket and processed individually. Initial currents of approximately 500 mA were measured. The dissolution current diminished gradually, as the amount of residual NiAl decreased. After approximately 12 h the current dropped to half the initial value; after approximately 38 h the current dropped to one tenth of the initial value. These values correspond to a nearly linear decrease in current over time. After approximately 55 h the current decay was complete – no further charge was consumed. The experiment was continued for several hours to ensure complete matrix dissolution. Finally, the solution was filtered using an ultra filtration unit and cellulose acetate filter papers with a nominal pore size of 200 nm (Sartorius AG, Göttingen, Germany).

An illustration of the number of wires that can be obtained was done by calculating the length of a virtual wire weighing 1 g. First the corresponding volume of tungsten V, considering the material' density of 19,250 kg m^{-3} [18] is calculated to be 5.19×10^{-8} m^3. Assuming an average wire diameter of 200 nm and the respective cross-sectional surface of 3.14×10^{-14} m^2, the length of a single wire with a diameter of 200 nm, weighing 1 g is 1653.5 km. Further, taking an average wire length of 300 μm the number of wires in 1 g is approximately 5.5 billion.

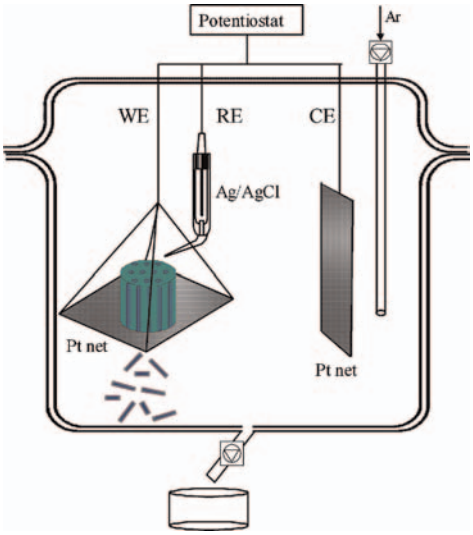

Figure 3 (online color at: www.pss-a.com) Schematic of the electrochemical cell applied in this work.

In order to verify the selectiveness of the dissolution process, analytical chemistry experiments were performed. Aliquot samples of the hydrochloric acid electrolyte were taken and analyzed using inductively coupled plasma optical emission spectrometry (ICP-OES). ICP-OES analyses were performed using a THERMO Iris Intrepid Duo HR. The filtrate showed small amounts of W (0.04 at.%). This value is well within the expected range of the solid solubility of W in NiAl, which is according to the phase diagram ~0.2 at.% [20]. Similarly, a significant amount of filtered W wires was investigated after alkaline pulping yielding residual contents of 0.17 and 1.38 at.% for Ni and Al, respectively. These relatively high values are assumed to result from residual matrix pieces within the filtrate, as can be seen in Fig. 4B (on the left, above the scale marker).

3.2 TEM analysis Using the Kleindiek manipulators, single wires were transferred to transmission electron microscopic (TEM) grid substrates for further investigation of the material properties. Due to their relatively high density the refractory metal nanowires were not suited for TEM; even the thinnest tungsten nanowires with diameters under 200 nm were not transmissive for the electron beam.

In order to overcome this problem another attempt was launched using the Kleindiek manipulators in combination with the focused ion beam (FIB) and gallium ion sputtering (GIS) systems. Wires were taken from a filter paper substrate using a Picoprobe needle mounted to a Kleindiek manipulator. The Zeiss/Leo 1540 XB is only equipped with one Kleindiek manipulator, therefore the wires had to be "glued"

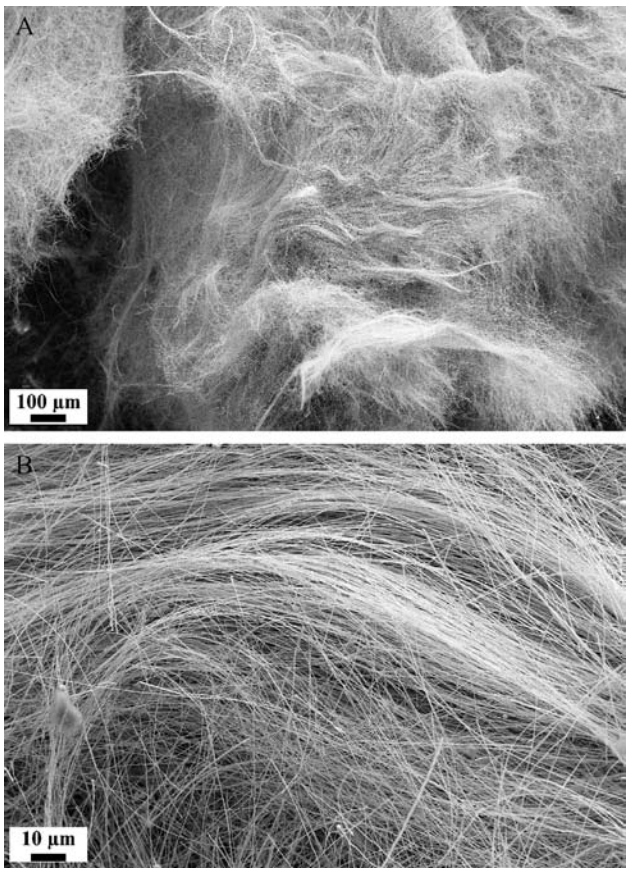

Figure 4 Large amounts of extreme aspect-ratio W nanowires. (A) A surface of approximately 1 mm^2 covered by nanowires. (B) Close-up view of W nanowires.

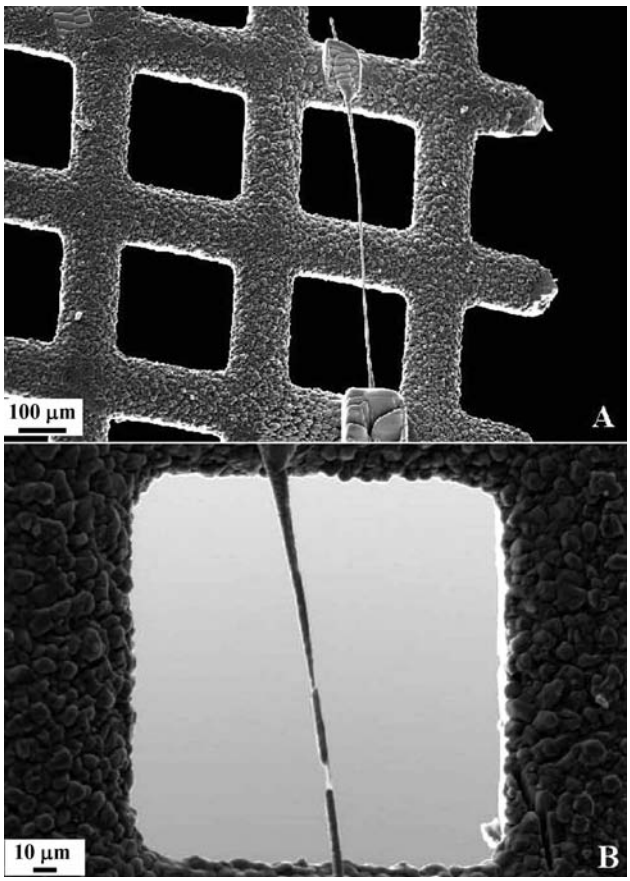

Figure 5 Tungsten wire placed on a copper TEM grid substrate using a Kleindiek nanomanipulator. (A) The wire was fixed in place by depositing platinum "pads." (B) Milling the wire with the FIB yielded thinned sections of the wire.

to the needle by depositing platinum. Next, the needle was lifted up and the substrate replaced with a copper grid. After placing the wire on the grid it was "glued" to this new substrate by depositing platinum. Then the wire was cut away from the needle using the ion beam. The adjacent end of the wire was "glued" to the substrate by depositing more platinum (Fig. 5A). Finally the GIS nozzle was retracted and the ion beam was used to thin the sample (Fig. 5B).

After mounting the tungsten nanowire to the copper grid, the sample was transferred to the TEM. A close-up view of the wire is shown in Fig. 6A. At first glance it is clear that the wire has a phase boundary along the middle – a white stripe along the entire sample. Energy dispersive X-ray (EDX) measurements were performed in order to ascertain the composition of both phases. The results of the EDX measurements are shown in Fig. 6B. From these results it is very clear that the upper part of the sample in Fig. 6A is tungsten, while the lower part consists of a mixture of copper, carbon, gallium, and platinum. The latter three elements can all be attributed to the FIB treatment: gallium ions are used to mill the samples and to decompose the carbon-containing precursor materials for depositing platinum. While thinning the wire, the ion beam was pointed at the copper substrate. Therefore, it is very likely that milled copper redeposited on the sample.

The crystallinity of the sample was determined using selected area diffraction (SAD). The selected area is shown in Fig. 7 ("spot" size 300 nm). Therefore, the result shown in Fig. 7C reflects both phases: the single crystalline tungsten yields a diffraction pattern consisting of an array of bright dots, while the deposited phase is polycrystalline and yields ring shaped diffraction patterns. In order to determine the crystallographic orientation of the wire convergent beam electron diffraction (CBED) was applied.

This technique utilizes a much smaller spot than SAD. The spot size in these experiments was 70 nm. CBED measurements were performed at four separate places along a 20 µm section of the tungsten wire under investigation. All recorded diffraction patterns indicate that the wire has an orientation close to ⟨001⟩ along the wire's growth direction.

It should be mentioned here that applying electron backscatter diffraction (EBSD) to polished cross-sections of directionally solidified samples is a more convenient way of determining the wires crystallographic orientation [21]. Of course, this is only possible prior to releasing the wires from the matrix. The TEM results showed that the tungsten wire is

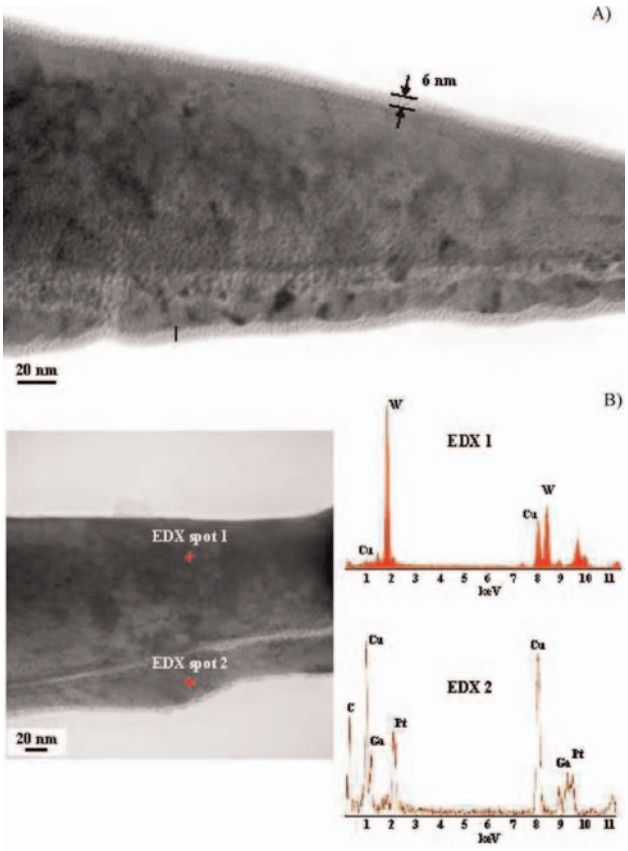

Figure 6 (online color at: www.pss-a.com) High resolution TEM image of the tungsten nanowire. (A) A close-up view and (B) EDX spot measurements.

single crystalline. The wire is covered by a very thin oxide layer, visible as the light colored layer in Fig. 6A (thickness approximately 6 nm), although no oxygen was found in the EDX spectra, which is in good agreement with passivation studies of nanoscopic tungsten. This is not surprising, as the EDX typically probes a relatively large volume. The interaction of the electron beam with the material reaches depths of up to 2–3 μm. Due to depth dependent probing probability the bulk signal can be assumed to result from an interaction depth of 1 μm. The oxide thickness comprises only 0.6% of that depth. When considering the stochiometry of the oxide (WO_3) and the fact that the heavier tungsten atoms will interact more strongly with the electron beam, 50% of the signal might be attributed to oxygen. Consequently, the amount of detectable oxygen is approximately 0.3% of the probed volume, while the detection limit of the EDX is above 1%. Therefore, it is plausible that the amount of oxygen probed is too small to be detected by the EDX detector.

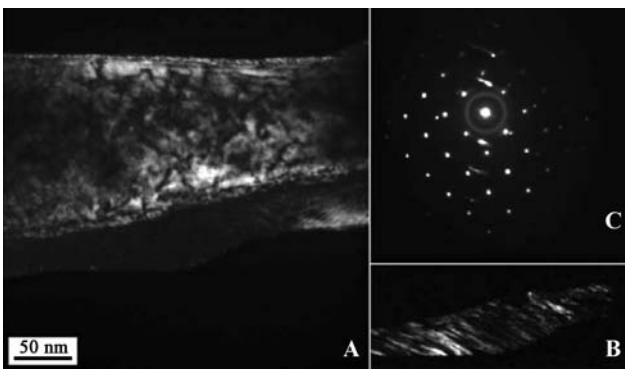

Figure 7 TEM investigation of the tungsten nanowire. (A) DF image of the tungsten wire. (B) DF image of the carbon, gallium, and platinum deposits. (C) SAD pattern showing two phases. Dots indicating a single crystalline tungsten phase and rings indicating a polycrystalline phase.

The EDX-spectra show no nickel or aluminium from the matrix phase present in the wires. Again, the probes sample volume must be compared to the (expected) amount of material. Theoretical considerations based on the phase diagram of the system as well as chemical trace analysis show that the amount of matrix material in the wire phase is very small. Thus, no traces of nickel or aluminum were found in the tungsten wires using EDX.

4 Summary Single crystalline tungsten nanowires were successfully synthesized at a large scale in laboratory conditions. Directional solidification and electrochemical processing of 21.3 g of NiAl-W eutectic alloy yielded 1 g of tungsten nanowires. This amount is equivalent to 5.5 billion of 300 μm long and 200 nm in diameter nanowires. Beside being monocrystalline, the nanowires exhibit extreme aspect ratios >1000 as well. High resolution TEM analysis proved their crystallinity, whereas EDX measurements showed that the nanowires consist of pure tungsten. In addition, it was observed that they are covered with a thin oxide layer with an estimated thickness of ∼6 nm. However, such a thin oxide layer could not be identified with EDX and further studies using Auger spectroscopy are being carried out to confirm the layer thickness.

Possible applications for these high aspect ratio, single crystal nanowires include pH-sensing [22], gas sensing [23–25], STM-probing [26, 27], as components in composite materials with low percolation thresholds, as electrode materials [28, 29], as field emitters [30–32] and for fabricating NEMS [21]. Finally, high temperature nanotechnology is possible as well (sources for polarized infra red light).

Acknowledgements Financial support of the Deutsche Forschungsgemeinschaft within the frame of the priority program "Nanowires and Nanotubes" project number HA 3118/4-3 is gratefully acknowledged.

References

[1] J. T. L. Thong, C. H. Oon, M. Yeadon, and W. D. Zhang, Appl. Phys. Lett. **81**, 4823 (2002).
[2] P. Liu, F. Arai, and T. Fukuda, Nanotechnology **17**, 3023 (2006).
[3] A. B. H. Tay and J. T. L. Thong, Appl. Phys. Lett. **84**, 5207 (2004).

[4] K. S. Yeong, J. B. K. Law, and J. T. L. Thong, Appl. Phys. Lett. **88**, 5207 (2006).
[5] Y. Li, X. Li, Z. X. Deng, B. Zhou, S. Fan, J. Wang, and X. Sun, Angew. Chem. Int. Ed. **41**, 333 (2002).
[6] J. Wang and Y. Li, Adv. Mater. **15**, 445 (2003).
[7] Z. Q. Liu, K. Mitsuishi, and K. Furuya, J. Appl. Phys. **96**, 619 (2004).
[8] Z. Q. Liu, K. Mitsuishi, and K. Furuya, J. Appl. Phys. **96**, 3983 (2004).
[9] S. Wang, Y. He, J. Zou, Y. Jiang, J. Xu, B. Huang, C. T. Liu, and P. K. Liaw, J. Cryst. Growth **306**, 433 (2007).
[10] Y. H. Lee, C. H. Choi, Y. T. Jang, E. K. Kim, B. K. Ju, N. K. Min, and J. H. Ahn, Appl. Phys. Lett. **81**, 745 (2002).
[11] I. M. Ross, I. J. Luxmoore, A. G. Cullis, J. Orr, P. D. Buckle, and J. H. Jefferson, J. Phys. **26**, 363 (2006).
[12] A. W. Hassel, B. Bello-Rodriguez, S. Milenkovic, and A. Schneider, Electrochim. Acta **51**, 795 (2005).
[13] A. W. Hassel, B. Bello-Rodriguez, S. Milenkovic, and A. Schneider, Electrochim. Acta **50**, 3033 (2005).
[14] A. W. Hassel, A. J. Smith, and S. Milenkovic, Electrochim. Acta **52**, 1799 (2006).
[15] S. Milenkovic, A. W. Hassel, and A. Schneider, Nano Lett. **6**, 794 (2006).
[16] M. Pourbaix, Atlas of Electrochemical Equilibria in Aqueous Solutions (Pergamon Press Ltd., Oxford, 1966).
[17] S. Milenkovic and A. W. Hassel, Phys. Status Solidi A **206**, 495 (2009).
[18] M. Winter, WebElements Periodic Table (The University of Sheffield and WebElements Ltd., UK, 1993–2009), www.webelements.com.
[19] A. W. Hassel, K. Fushimi, and M. Seo, Electrochem. Commun. **1**, 180 (1999).
[20] Z. M. Alekseeva, Handbook of Ternary Alloy Phase Diagrams (ASM International, Materials Park, Ohio, 1995).
[21] V. Cimalla, C. C. Röhlig, J. Pezoldt, M. Niebelschütz, O. Ambacher, K. Brückner, M. Hein, J. Weber, S. Milenkovic, A. J. Smith, and A. W. Hassel, J. Nanomater. **2008**, 638947 (2008).
[22] C. Fenster, A. J. Smith, A. Abts, S. Milenkovic, and A. W. Hassel, Electrochem. Commun. **10**, 1125 (2008).
[23] J. Polleux, A. Gurlo, N. Barsan, U. Weimar, M. Antonietti, and M. Niederberger, Angew. Chem. Int. Ed. **45**, 261 (2006).
[24] Y. S. Kim, S. C. Ha, and K. Kim, Appl. Phys. Lett. **86**, 213105 (2005).
[25] C. S. Rout, K. Ganesh, and A. Govindaraj, Appl. Phys. A **85**, 241 (2006).
[26] O. Kubo, Y. Shingaya, and M. Nakaya, Appl. Phys. Lett. **88**, 254101 (2006).
[27] A. B. H. Tay and J. T. L. Thong, Appl. Phys. Lett. **84**, 5207 (2004).
[28] S. J. Yoo, J. W. Lim, and Y. E. Sung, Appl. Phys. Lett. **90**, 173126 (2007).
[29] Z. J. Gu, H. Q. Li, and T. Y. Zhai, J. Solid State Chem. **180**, 98 (2007).
[30] K. Huang, Q. T. Pan, and F. Yang, Mater. Res. Bull. **43**, 919 (2008).
[31] J. P. Singh, F. Tang, and T. Karabacak, J. Vac. Sci. Technol. **22**, 1048 (2004).
[32] K. Huang, Q. T. Pan, and F. Yang, Physica E **39**, 219(2007).